Spectral signatures in satellite soil moisture reveal irrigation patterns across the contiguous United States

Christian Massari[1,*], Sara Modanesi[1], Zdenko Heyvaert[2,6], Louise Busschaert[2], Pierre Laluet[3], Martina Natali[1,2], Jacopo Dari[1,3], Luca Brocca[1], Wouter Dorigo[4], Clement Albergel[5], Gabriëlle De Lannoy[2]

[1] National Research Council, Perugia, Italy
[2] KU Leuven, Belgium
[3] University of Perugia, Italy
[4] TU Wien, Austria
[5] European Space Agency, UK
[6] ECMWF, UK

*Corresponding author: christian.massari@cnr.it

Preprint statement

This manuscript is a non-peer-reviewed preprint submitted to EarthArXiv. It has been submitted for peer review to *Geophysical Research Letters*.

Keywords: irrigation, soil moisture, wavelet analysis, remote sensing, SMOS, hydrology

March 2026

Spectral signatures in satellite soil moisture reveal irrigation patterns across the contiguous United States

Christian Massari[1], Sara Modanesi[1], Zdenko Heyvaert[2,6], Louise Busschaert[2], Pierre Laluet [3], Martina Natali[1,2], Jacopo Dari[1,3], Luca Brocca[1], Wouter Dorigo [4], Clement Albergel [5], Gabriëlle De Lannoy[2]

[1]National Research Council, Via Madonna Alta 126, Perugia, Italy
[2]Department of Earth and Environmental Sciences, KU-Leuven University, Leuven, Belgium
[3]Department of Civil and Environmental Engineering, University of Perugia, Italy
[4]Department of Geodesy and Geoinformation, TU WIEN, Vienna, Austria
[5]European Space Agency, ECSAT, Oxford, UK
[6]Research Department, ECMWF, Reading, UK

Key Points:

- Irrigation modifies the spectral characteristics of soil moisture.
- Spectral differences between SMOS observations and irrigation-off Noah–MP simulations detect irrigated areas.
- A SMOS-derived irrigation map improves the representation of irrigation patterns in Noah–MP simulations across the contiguous United States.

Corresponding author: Christian Massari, `christian.massari@cnr.it`

Abstract

Irrigation profoundly alters the terrestrial water cycle, yet its spatial distribution and temporal variability remain poorly constrained. Here, we introduce a new approach to detect irrigation in space based on spectral differences between modelled and satellite-observed soil moisture time series. Using wavelet decomposition, we isolate irrigation-induced variability at sub-annual scales by comparing Noah–MP simulations with and without irrigation. We then analyse differences between Soil Moisture and Ocean Salinity (SMOS) soil moisture retrievals and model simulations without irrigation to identify irrigated areas. We apply this method over the Contiguous United States (CONUS) for the period 2010–2023. Results show that irrigation enhances the power of seasonal and sub-seasonal spectral components of soil moisture, enabling identification of irrigated and non-irrigated areas when comparing observed and modelled soil moisture. Comparison with LGRIP30, an irrigation dataset for the United States, shows moderate-to-good agreement in the spatial patterns of irrigation. Major irrigated regions across CONUS largely coincide with those identified in LGRIP30, while discrepancies increase in areas with weaker irrigation signals or dense vegetation. The resulting SMOS-derived irrigation map suggests spatial patterns of irrigated areas that differ from those represented in static reference maps such as LGRIP30. When used to constrain Noah–MP simulations, SMOS-derived irrigation map highlights alternative irrigation distributions that better reflect actual irrigation spatial patterns and water use. Our method provides a scalable, all-weather pathway to detect where irrigation occurs, offering new observational constraints for representing irrigation in land and Earth-system models.

Plain Language Summary

Irrigation is essential for global food production, but we still do not know how much water is used for irrigation and how it varies over time and across regions. This limits our ability to understand the water cycle and to plan for sustainable water management. Satellite missions such as ESA's Soil Moisture and Ocean Salinity (SMOS) provide regular global measurements of soil moisture, which can reveal where irrigation is happening.

In this study, we analyzed SMOS soil moisture data together with computer model simulations to look at the "spectral fingerprint" of irrigation – the way it changes soil moisture patterns over time. Using a mathematical technique called wavelet analysis,

we isolated the portion of the signal most influenced by irrigation and trained a machine learning algorithm to identify irrigated areas.

Our results show that this approach can detect irrigation across the contiguous United States with good accuracy. This method can be applied globally, offering new opportunities to monitor irrigation and improve water management.

1 Introduction

Irrigation is one of the most significant human interventions in the terrestrial water cycle, yet its distribution and extent remain highly uncertain, limiting our ability to close the water balance and to represent land–atmosphere interactions in models (McDermid et al., 2023). Reliable global information on where and when irrigation occurs is challenging to obtain, and most land surface models rely on maps derived from subnational irrigation inventories that fail to capture its dynamic and heterogeneous nature (Neumann et al., 2011).

Satellite observations provide a unique opportunity to detect and quantify irrigation, using, for example, retrievals of soil moisture (Brocca et al., 2018), vegetation activity (Chiesi et al., 2022), evapotranspiration (Brombacher et al., 2022), and land surface temperature (Purnamasari et al., 2025), with near-global coverage and frequent revisit times (Massari et al., 2021). Specifically, some previous studies have attempted to detect and quantify irrigation by comparing satellite soil moisture retrievals with model outputs that exclude irrigation and analysing differences in their variability (Lawston et al., 2017; Zaussinger et al., 2019). However, despite promising results in certain regions, irrigation detection remains challenging due to uncertainties in the spatial footprint of satellite soil moisture retrievals and the presence of several confounding factors, including topography, heterogeneous vegetation cover, agricultural practices such as tillage, satellite signal disturbances such as radio frequency interference, and the often smaller spatial scale of irrigation relative to the satellite footprint.

Here we present a new method that exploits the spectral signature of irrigation in satellite soil moisture time series. Using wavelet decomposition, we isolate irrigation-driven variability at sub-annual scales and derive spectral features from the differences between simulations with and without irrigation. These features are used to train a random forest classifier on synthetic soil moisture time series generated with the Noah–MP land sur-

face model (Niu et al., 2011). The trained classifier is then applied to wavelet-transformed soil moisture observations from SMOS (Kerr et al., 2010) to detect irrigated areas across CONUS. By combining wavelet-based spectral analysis with a machine-learning classifier trained on synthetic land surface model simulations, the proposed framework enables irrigation detection directly from satellite soil moisture time series and reveals spatial patterns of irrigated areas that may differ from those represented in existing satellite- and inventory-based irrigation datasets, which often describe irrigation conditions for a single reference year.

2 Study area, methods and datasets

The analysis was conducted over CONUS, which spans a wide range of hydroclimatic regimes and irrigation intensities, providing an ideal testbed for irrigation detection methods. We used the ESA SMOS Level-2 soil moisture product (v700; European Space Agency (ESA) 2021) for the period 2010–2023. The product has an effective spatial resolution of approximately 43 km and is geolocated on the equal-area Icosahedral Snyder Equal Area (ISEA) 4H9 grid, with retrievals typically available every two to three days. Recommended quality flags were applied to filter out radio-frequency interference, poor retrievals, non-agricultural land, mountainous terrain, coastal areas, open water, and urban surfaces (see Section S1.1 of the Supplementary Information, SI). The SMOS observations were regridded to a regular 0.25° latitude–longitude grid (EPSG:4326) using nearest-neighbour interpolation and aggregated to weekly resolution. This grid is aligned with the Noah–MP model grid used in the simulations.

The Landsat-derived Global Rainfed and Irrigated Cropland product (LGRIP30; Teluguntla et al., 2023), shown in Figure S1 of the SI for the nominal year 2015, was used as a reference dataset to develop the method and evaluate the SMOS-based estimates of irrigated area. The original LGRIP30 maps have a spatial resolution of 30 m. To match the spatial resolution of the model simulations and SMOS observations, the dataset was aggregated to the same 0.25° (see SI section 1.3 for further details).Annual state-level irrigation volumes from the USDA Farm and Ranch Irrigation Survey (FRIS; Section S1.3 of the SI) for the years 2013 and 2018 were used as benchmark data for the Noah–MP simulations of irrigation amounts.

Soil moisture estimates were obtained with the Noah–MP land surface model (v4.0.1; Niu et al., 2011) implemented in the NASA Land Information System (S. V. Kumar et al., 2006; Peters-Lidard et al., 2007). The model was run on the same regular 0.25° grid as the reprocessed SMOS data and forced with ERA5 forecast fields (Hersbach et al., 2020). Two deterministic Noah–MP simulations were performed with and without the dynamic sprinkler irrigation module (Ozdogan et al., 2010) (hereafter irrigation-on and irrigation-off simulations) using static maps of irrigated fraction from LGRIP30 and climatological green vegetation fraction seasonality. These simulations provide synthetic soil-moisture time series used for the wavelet analysis and for training the irrigation detection method.

The irrigation detection model developed in this study was then applied to SMOS observations to derive a satellite-based map of irrigated areas. This SMOS-derived irrigation map was subsequently used to constrain Noah–MP ensemble simulations with perturbed meteorological forcings to estimate irrigation volumes. A parallel ensemble simulation forced with the original LGRIP30 irrigation map was also performed for comparison. A detailed description of the Noah–MP model setup, irrigation scheme parameters, and simulation experiments is provided in the Supplementary Information (Sections S1.4–S1.5).

We applied a Continuous Wavelet Transform (CWT; Section S1.6) using a Morlet mother wavelet (Torrence & Compo, 1998) to decompose weekly soil-moisture time series into time–frequency space and compute global wavelet power spectra for Noah–MP irrigation-on and irrigation-off simulations and for SMOS observations. Wavelet differences were computed between Noah–MP irrigation-on and irrigation-off soil moisture time series to train the classification method, and between Noah–MP irrigation-off simulations and SMOS soil moisture observations (Section S1.6.2) to detect irrigation under real-world conditions. Two metrics were derived from the wavelet analysis (Section S1.6.5): (i) the bias in the global wavelet power spectrum (M_p), computed as the difference between an irrigated signal (either Noah–MP irrigation-on or SMOS observations over a candidate irrigated area) and the corresponding Noah–MP irrigation-off simulation, averaged over the 6–18-month period band; and (ii) the reduction in wavelet coherence (M_C), defined as $M_C = 1 - \overline{R^2}_{B_C}$, where $\overline{R^2}_{B_C}$ is the wavelet coherence averaged over the same 6–18-month band between the two signals. The 6–18-month period range was selected to capture irrigation-driven modifications of the seasonal soil-moisture cycle while minimiz-

ing sensitivity to high-frequency retrieval noise at shorter periods and edge effects and low-frequency hydroclimatic variability at longer periods.

A Random Forest classifier (RFC; Breiman, 2001) was trained on wavelet-derived spectral features from simulated irrigation-on and irrigation-off soil moisture time series to classify pixels as irrigated or non-irrigated (Section S1.7 of the SI). The LGRIP30 irrigation map was used as the target variable during training. Because the classifier is trained only on spectral features derived from synthetic simulations and does not use geographic information, it cannot learn location-specific irrigation patterns from LGRIP30, ensuring that its application is independent of location. To construct the training dataset, additional predictors and perturbations were introduced. For each grid cell we computed the aridity index (AI), defined as the ratio of potential evapotranspiration to precipitation from ERA5 forecast fields. Binary irrigation labels were assigned using thresholds of LGRIP30 irrigated fraction (10%, 20%, 30%, and 40% of total area). To account for discrepancies between satellite observations and model simulations when applying the classifier to SMOS data, Gaussian noise with zero mean and standard deviations between 5% (representing typical satellite soil-moisture uncertainty; Karthikeyan et al., 2017) and 30% (worst-case scenario) was added to the simulated soil-moisture time series. These perturbations represent the combined uncertainty arising from retrieval noise, model structural errors, and parameter uncertainty and, in general, do not reflect the accuracy of the SMOS observations. The trained RFC was then applied to spectral differences between SMOS soil moisture observations and irrigation-off Noah–MP simulations.

The Receiver Operating Characteristic Curve (ROC) and the Area Under the Curve (AUC) were used to assess the classification performance (Fawcett, 2006; Hanley & McNeil, 1982) for different thresholds on the irrigated area fraction and different noise levels applied to the simulated irrigated soil-moisture time series, using LGRIP30 as a comparison dataset. Although LGRIP30 does not represent ground truth, it provides a realistic, high-resolution reference for evaluating the similarity of the spatial patterns identified by our approach. The SMOS-derived binary irrigation maps were then scaled using the LGRIP30 irrigation fractions to constrain Noah–MP simulations of irrigation amounts. This scaling is necessary because the SMOS classification determines the binary spatial pattern of irrigated areas, while the LGRIP30 irrigation fraction constrains the total irrigated area within each 0.25° grid cell, thereby preserving the SMOS-derived spatial dis-

tribution. The resulting irrigation simulations (SMOS-derived) and simulations using the original LGRIP30 irrigation map were evaluated against FRIS data.

Additional methodological details are provided in the SI, and a schematic overview of the workflow is shown in Figure 1.

3 Results

To illustrate the expected differences in wavelet spectra between irrigation-on and irrigation-off soil moisture time series, examples are shown for locations without and with irrigation. In non-irrigated regions, the wavelet power spectra of SMOS and Noah–MP (irrigation-off) are characterized by a dominant annual peak, and the bias near the 12-month period approaches zero, indicating similar spectral content typical of rain-fed systems (Figure 2a; Figure S2). In contrast, irrigated regions exhibit a reduced contrast between the annual and semiannual peaks, with semiannual power approaching the magnitude of the annual cycle (Figure 2b; Figure S3). This pattern reflects additional wetting events associated with irrigation that are superimposed on the seasonal precipitation cycle. This spectral shift is accompanied by a marked reduction in wavelet coherence between SMOS and the irrigation-off Noah-MP simulation at 6–18-month periods (Figure 2d), compared to non-irrigated areas (Figure 2c). The loss of coherence indicates that irrigation introduces variability not captured by the model when irrigation is disabled. The selected range of scales minimizes the influence of high-frequency noise in the satellite retrievals and edge effects affecting both weekly variability and periods longer than approximately two years. Overall, the spectral approach offers a clear advantage over direct inspection of raw soil moisture time series by isolating irrigation-related low-frequency variability from high-frequency observational noise, enabling a more robust discrimination between irrigated and non-irrigated systems (see Figure S3b).

While the bias and coherence-drop metrics can be inspected at individual locations, mapping irrigation consistently across CONUS requires a generalized framework. The wavelet-based metrics derived from Noah–MP irrigation-on and irrigation-off simulations were therefore used to train the RFC to distinguish irrigated from non-irrigated conditions (see Methods). The spatial distributions of the predictor variables used by the classifier, including aridity index (AI), wavelet power bias, and coherence reduction (M_C), are shown in Figure S4 of the SI. A clear pattern of increasing wavelet power bias is ob-

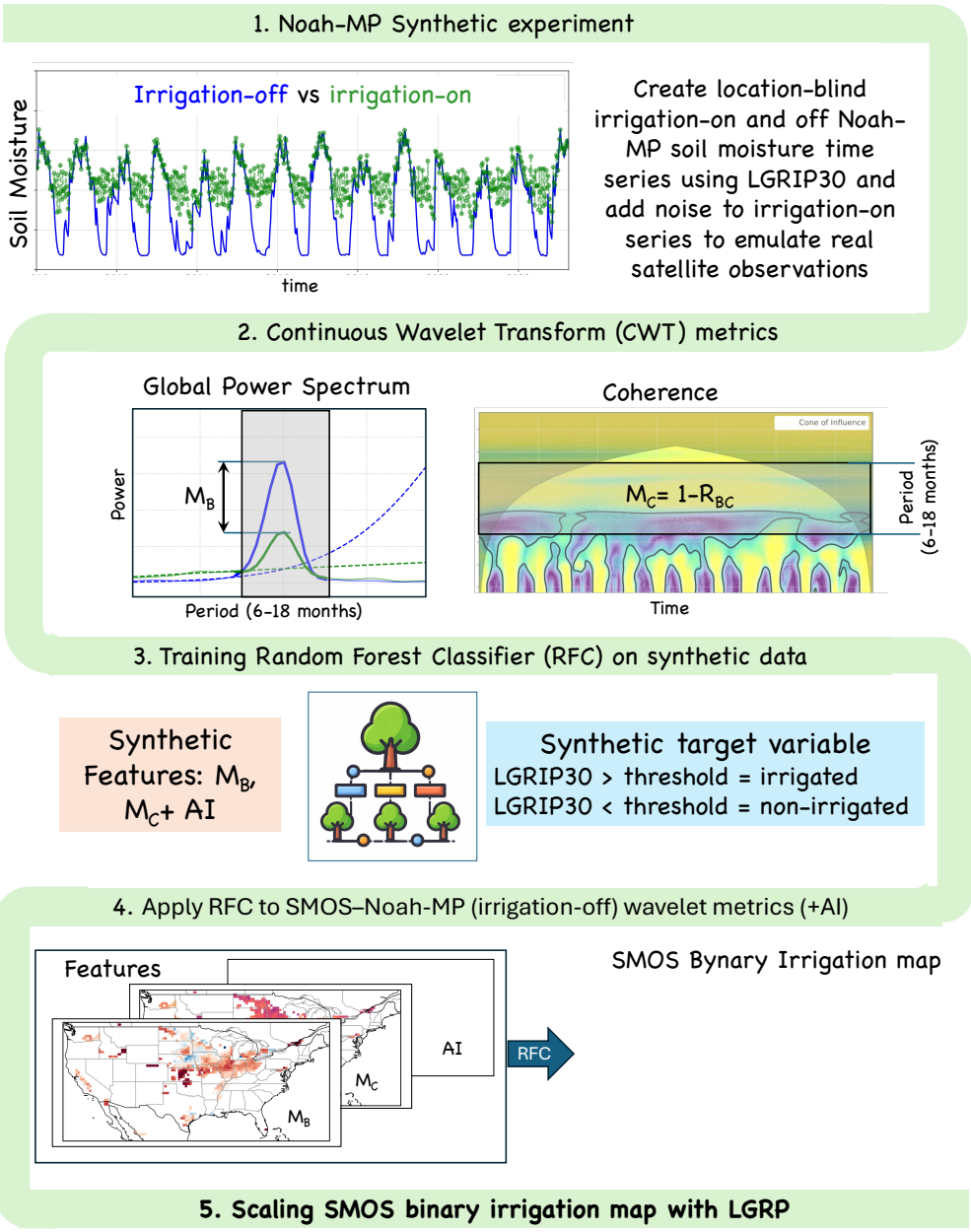

Figure 1. Schematic overview of the wavelet-based irrigation detection framework. (1) Synthetic soil-moisture (SM) time series are generated using the Noah–MP land surface model with irrigation-on and irrigation-off based on irrigation fractions from the Landsat-derived Global Rainfed and Irrigated Cropland product (LGRIP30). Multiple noise levels are added to the synthetic time series to emulate combined satellite retrieval uncertainty and model–data discrepancies. (2) A Continuous Wavelet Transform (CWT) is applied to paired soil moisture time series to compute the global wavelet power spectrum and wavelet coherence. From these spectra, irrigation-sensitive metrics are derived over the 6–18 month period range, including the bias in wavelet power and the reduction in wavelet coherence relative to simulations without irrigation. (3) A Random Forest classifier (RFC) is trained on synthetic experiments using aridity index (AI), wavelet power bias (M_B), and coherence reduction (M_C) as predictor variables and binary irrigation labels derived from LGRIP30 as targets (Section SI S1.6.5). (4) The trained RFC is applied to CWT-derived features from Soil Moisture and Ocean Salinity (SMOS) satellite observations and Noah–MP simulations irrigation-off to produce maps of irrigated and non-irrigated areas, (5) the binary classification map is scaled by LGRIP30. Wavelet spectra and coherence panels are shown schematically for illustration.

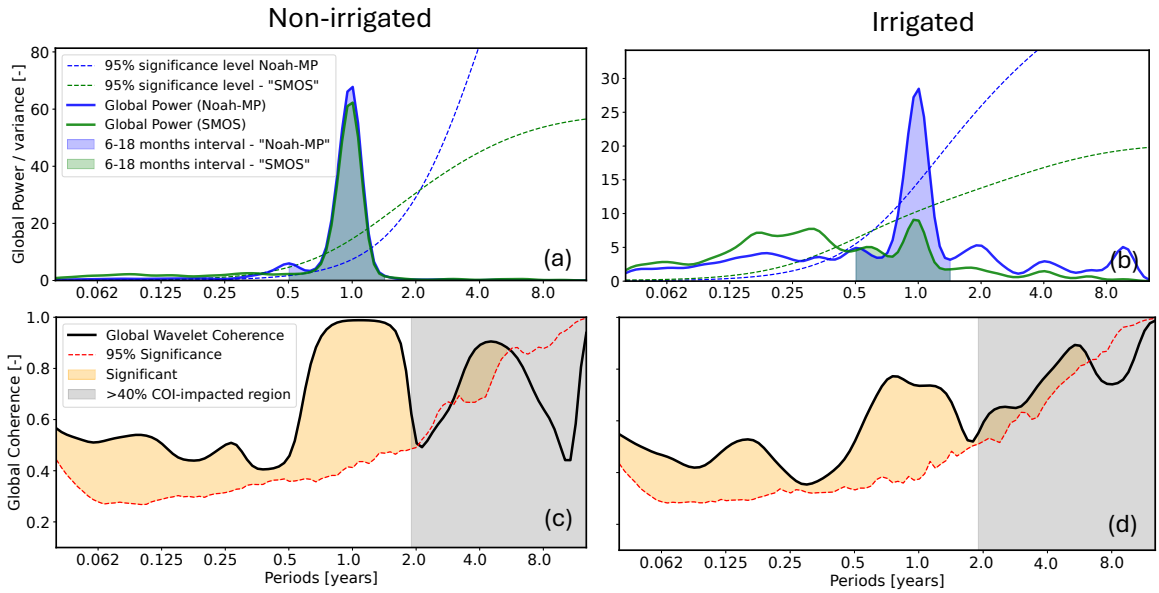

Figure 2. (a,b) Global wavelet power spectra of surface soil moisture from Noah-MP (irrigation-off) and SMOS for (a) a non-irrigated pixel in Eastern Washington (irrigation fraction $<$ 10% according to LGRIP30) and (b) an irrigated pixel in South Dakota (irrigation fraction $\approx$ 80%). Dashed lines indicate the 95% significance levels relative to a red-noise background spectrum, following Torrence & Compo (1998). Thick lines highlight the 6–18-month period range used for the derivation of wavelet-based irrigation metrics. (c,d) Corresponding global wavelet coherence between Noah-MP (irrigation off) and SMOS for the same non-irrigated (c) and irrigated (d) pixels. The red dashed line denotes the 95% significance level based on Monte Carlo simulations assuming red noise (Torrence & Compo, 1998; Grinsted et al., 2004). Gray shading marks periods where more than 40% of the signal is affected by the cone of influence (COI).

served over intensively irrigated regions, along with a general north–south gradient in M_C, indicating reduced coherence over irrigated regions.

The SMOS-derived irrigation map obtained using a 20% irrigation-fraction threshold and assuming a noise level of 20% is shown in Figure 3. In this configuration, the SMOS classification determines the spatial pattern of irrigated areas, while the LGRIP30 dataset constrains the irrigated fraction within each grid cell. Comparison with the LGRIP30 product (Figure S1) indicates that the major irrigated regions of CONUS, including California's Central Valley, Washington State, the central–southern United States, and the Great Plains, are well captured by the wavelet-based approach. Local discrepancies are observed in areas with lower irrigated fractions, particularly within portions of the Great Plains, where irrigation signals are weaker. Agreement between the two datasets also decreases in colder climates, where the seasonal overlap between precipitation and irrigation reduces the distinctiveness of the spectral signature, and in the Corn Belt, where dense vegetation may degrade the SMOS soil-moisture retrievals. Similar patterns of agreement and discrepancy over CONUS have been reported in previous studies (Zaussinger et al., 2019; S. Kumar et al., 2015; Crow et al., 2025).

A quantitative comparison with the LGRIP30 reference, assuming irrigated pixels where LGRIP30 $\geq 20\%$, yields an AUC of 0.7, indicating moderate agreement between the SMOS-based classification and the binary LGRIP30 irrigation map. The corresponding confusion matrix and the spatial distribution of true positives, true negatives, false positives, and false negatives are provided in the SI (Table S2 and Figures S6). Sensitivity analyses exploring alternative irrigation-fraction thresholds and noise assumptions are also reported in the SI Figure S7. These analyses show that lower noise levels and smaller irrigation thresholds generally lead to reduced agreement (Section S2.1).

To assess whether the SMOS-derived irrigation map improves the representation of irrigation volumes across CONUS, we compared Noah–MP irrigation estimates obtained using the original LGRIP30 irrigation fractions (Figure S8) with those derived from the SMOS-based irrigation map scaled by LGRIP30 within each 0.25° grid cell (Figure S8b). Simulated irrigation volumes were aggregated at the state level and evaluated against irrigation statistics from the USDA Farm and Ranch Irrigation Survey (FRIS; see SI Section S1.3).

Results (Figure S9) show consistently higher Pearson correlation coefficients when using the SMOS-based configuration than when using LGRIP30 directly. Correlation coefficients between country-aggregated irrigation levels from FRIS and our simulations are $R = 0.92$ in both years with the SMOS-based approach, compared with $R = 0.81$ in 2013 and $R = 0.78$ in 2018 for the LGRIP30-based configuration. Bias magnitudes are comparable between the two approaches but with opposite signs, with mean bias values of -2.05 km^{3}yr^{-1} for the SMOS-based configuration and 2.07 km^3, yr^{-1} for the LGRIP30-based configuration, while RMSD values are similar (4.55 and 4.58 km^{3}yr^{-1}, respectively). These results indicate that incorporating the SMOS-based irrigation classification improves the representation of irrigation volumes in Noah–MP simulations. Additional details of this analysis and the irrigation maps used in the simulations are provided in Section S2.2 of the SI.

Conclusions

We presented a new method to detect irrigation based on the spectral analysis of soil moisture time series. Using wavelet decomposition, we isolated irrigation-driven variability at sub-annual scales and quantified two key metrics: the bias in wavelet power spectra and the reduction in wavelet coherence between SMOS observations and irrigation-off Noah–MP simulations.

By training a Random Forest classifier on synthetic soil-moisture time series simulated with and without irrigation using Noah–MP, and by introducing different noise levels in the irrigation-on soil moisture signals and applying multiple thresholds to the LGRIP30 irrigation fractions to define binary irrigation labels, we generalized the relationship between wavelet-based metrics, AI, and irrigation presence. Applied to SMOS observations and irrigation-off Noah–MP simulations over CONUS, the method successfully mapped major irrigated regions, including California's Central Valley, the High Plains, and parts of the southeastern United States. Comparison against the LGRIP30 product yielded an AUC of 0.7, demonstrating moderate-to-good discrimination despite model and retrieval uncertainties. Additionally, Noah–MP simulations constrained by the new SMOS-derived irrigation map improve the spatial representation of state-level irrigation water use across CONUS. The SMOS-based classification therefore provides an alternative irrigation map derived from multi-year SMOS soil moisture observations, complementing static reference datasets such as LGRIP30.

The approach relies on land surface model simulations without irrigation to provide a reference representation of rain-fed soil moisture dynamics. In this study Noah–MP was used for this purpose, but the framework is not tied to a specific model and could be applied with other land surface models capable of simulating soil moisture variability under rain-fed conditions.

This approach offers a scalable framework for irrigation detection at continental to global scales. The method is currently limited by the coarse resolution of the SMOS data and primarily complements existing methods based on higher-resolution optical observations. Future work will focus on characterizing the timing and intensity of irrigation by exploiting the full wavelet spectrum and integrating higher-resolution observations from current and upcoming radar missions such as ROSE-L and NISAR. More generally, the framework is flexible and could potentially be applied using other types of input variables that act as proxies for irrigation signals, provided that they capture irrigation-induced anomalies in land surface conditions.

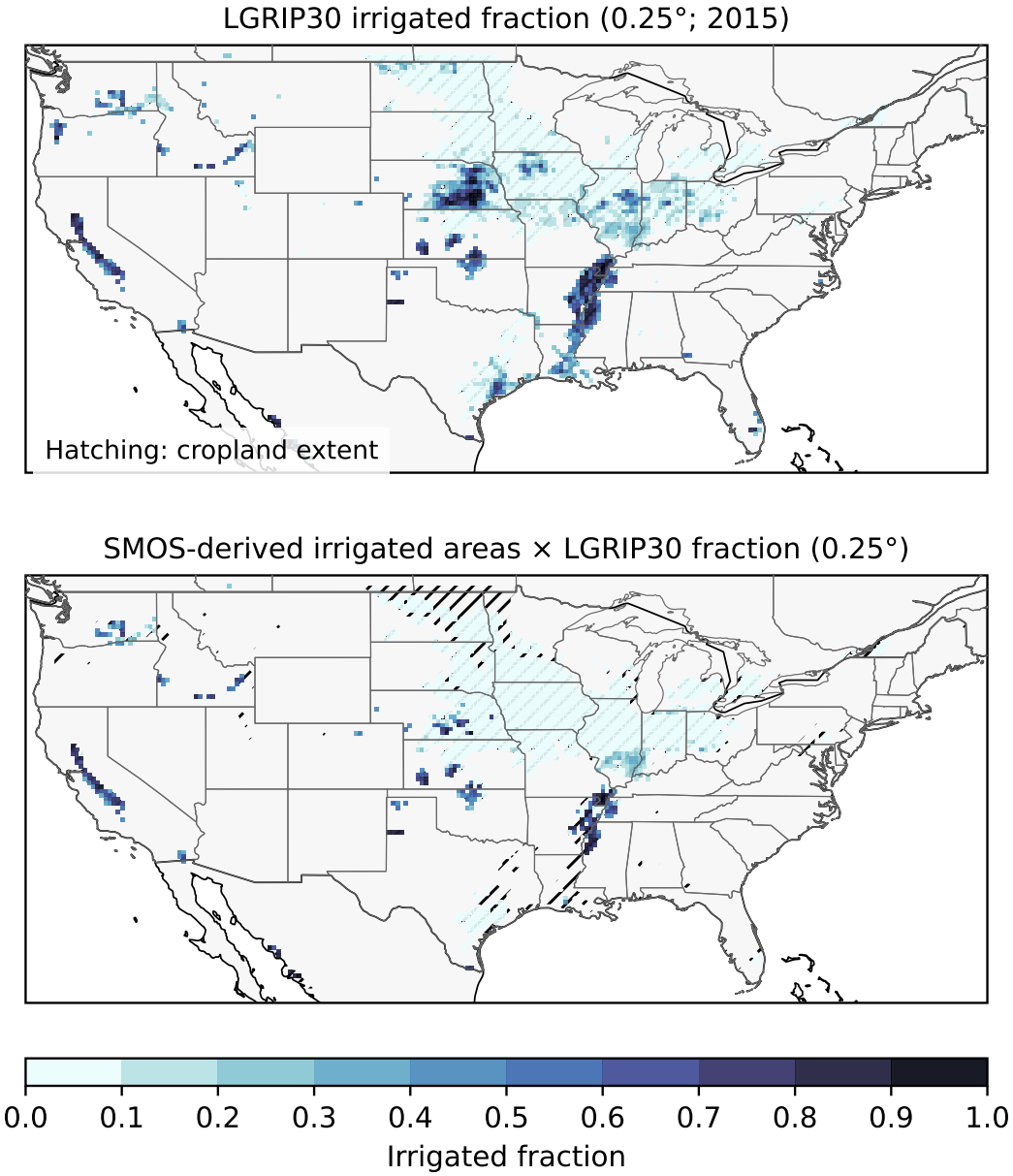

Figure 3. Irrigated fraction maps on the 0.25° grid over the Contiguous United States (CONUS). (a) Irrigated fraction from the Landsat-derived Global Rainfed and Irrigated Cropland product (LGRIP30; nominal year 2015) aggregated to the model grid. (b) Irrigated fraction obtained by combining the SMOS-based binary irrigation classification (20% threshold) with the LGRIP30 irrigated fraction within each grid cell. In this configuration, the SMOS classification determines the spatial pattern of irrigated areas, while the LGRIP30 fraction constrains the irrigated area within each 0.25° grid cell. Hatching indicates cropland extent. The color scale shows irrigated fraction divided into ten equal intervals between 0 and 1.

Open Research Section

SMOS Level–2 soil moisture data are publicly available from the European Space Agency (ESA) Earth Online portal (`https://earth.esa.int/eogateway`). ERA5 atmospheric forcing data were obtained from the Copernicus Climate Data Store (`https://cds.climate.copernicus.eu`). The Landsat-derived Global Rainfed and Irrigated Cropland product (LGRIP30) is publicly available from the NASA Land Processes Distributed Active Archive Center (LP DAAC). State-level irrigation statistics from the USDA Farm and Ranch Irrigation Survey (FRIS) are available from the U.S. Department of Agriculture (`https://www.nass.usda.gov`).

Noah–MP simulations were performed using the NASA Land Information System (LIS), which is publicly available at `https://lis.gsfc.nasa.gov`. The scripts used to perform the wavelet analysis and Random Forest classification, together with the derived irrigation classification maps and supporting diagnostics, will be deposited in a public repository (e.g., Zenodo), and a persistent DOI will be provided upon acceptance.

Acknowledgments

This work was supported by the European Space Agency (ESA) Climate Change Initiative Anthropogenic Water Use (CCI-AWU, `https://climate.esa.int/en/projects/anthropogenic-water-use/`) project. The authors thank the ESA CCI programme for providing the framework and support that enabled this research. Louise Busschaert is funded by Fonds Wetenschappelijk Onderzoek (FWO) grant 1158423N.

References

Breiman, L. (2001). Random forests. , *45*(1), 5–32. Retrieved 2025-09-01, from `https://doi.org/10.1023/A:1010933404324` doi: 10.1023/A:1010933404324

Brocca, L., Tarpanelli, A., Filippucci, P., Dorigo, W., Zaussinger, F., Gruber, A., & Fernández-Prieto, D. (2018). How much water is used for irrigation? a new approach exploiting coarse resolution satellite soil moisture products. *International journal of applied earth observation and geoinformation*, *73*, 752–766.

Brombacher, J., de Oliveira Silva, I. R., Degen, J., & Pelgrum, H. (2022). A novel evapotranspiration based irrigation quantification method using the hydrological similar pixels algorithm. *Agricultural Water Management*, *267*, 107602.

Chiesi, M., Angeli, L., Battista, P., Fibbi, L., Rapi, B., Gozzini, B., & Maselli, F. (2022). Monitoring and analysis of crop irrigation dynamics in central italy through the use of modis ndvi data. *European Journal of Remote Sensing*, *55*(1), 23–36.

Crow, W. T., Anderson, M. C., Volk, J. M., & Colliander, A. (2025). Value of microwave soil moisture and thermal-infrared evapotranspiration retrievals for the mapping of irrigation coverage. *International Journal of Applied Earth Observation and Geoinformation*, *143*, 104773.

European Space Agency (ESA). (2021). *SMOS L2 SM V700 (and L1 V724) science data.* doi: 10.57780/SM1-857c3d7

Fawcett, T. (2006). An introduction to roc analysis. *Pattern Recognition Letters*, *27*(8), 861–874. doi: 10.1016/j.patrec.2005.10.010

Grinsted, A., Moore, J. C., & Jevrejeva, S. (2004). Application of the cross wavelet transform and wavelet coherence to geophysical time series. , *11*(5), 561–566. Retrieved 2025-09-22, from `https://npg.copernicus.org/articles/11/561/2004/` (Publisher: Copernicus GmbH) doi: 10.5194/npg-11-561-2004

Hanley, J. A., & McNeil, B. J. (1982). The meaning and use of the area under a receiver operating characteristic (roc) curve. *Radiology*, *143*(1), 29–36. doi: 10.1148/radiology.143.1.7063747

Hersbach, H., Bell, B., Berrisford, P., Hirahara, S., Horányi, A., Muñoz-Sabater, J., ... Thépaut, J.-N. (2020). The era5 global reanalysis. *Quarterly Journal of the Royal Meteorological Society*, *146*(730), 1999-2049.

Karthikeyan, L., Pan, M., Wanders, N., Kumar, D. N., & Wood, E. F. (2017). Four decades of microwave satellite soil moisture observations: Part 2. product validation and inter-satellite comparisons. *Advances in Water Resources*, *109*, 236–252.

Kerr, Y. H., Waldteufel, P., Wigneron, J.-P., Delwart, S., Cabot, F., Boutin, J., ... Mecklenburg, S. (2010). The SMOS mission: New tool for monitoring key elements ofthe global water cycle. , *98*(5), 666–687. Retrieved 2025-09-01, from `https://ieeexplore.ieee.org/document/5446359` doi: 10.1109/JPROC.2010.2043032

Kumar, S., Peters-Lidard, C., Santanello, J., Reichle, R. H., Draper, C., Koster, R. D., ... Jasinski, M. F. (2015). Evaluating the utility of satellite soil moisture retrievals over irrigated areas and the ability of land data assimilation methods to

correct for unmodeled processes. *Hydrology and Earth System Sciences*, *19*(11), 4463–4478.

Kumar, S. V., Peters-Lidard, C. P., Tian, Y., Houser, P., Geiger, J., Olden, S., ... Sheffield, J. (2006). Land information system: An interoperable framework for high resolution land surface modeling. *Environ. Model. Softw.*, *21*, 1402–1415.

Lawston, P. M., Santanello, J. A., & Kumar, S. V. (2017). Irrigation signals detected from SMAP soil moisture retrievals. , *44*(23), 11,860–11,867. Retrieved 2021-08-25, from https://agupubs.onlinelibrary.wiley.com/doi/abs/10.1002/2017GL075733 (_eprint: https://agupubs.onlinelibrary.wiley.com/doi/pdf/10.1002/2017GL075733) doi: 10.1002/2017GL075733

Massari, C., Modanesi, S., Dari, J., Gruber, A., de Lannoy, G., Girotto, M., ... Zribi, M. (2021). A review of irrigation information retrievals from space and their utility for users. , *13*(20). Retrieved from https://www.scopus.com/inward/record.uri?eid=2-s2.0-85110745042&doi=10.3390%2Frs13204112&partnerID=40&md5=c46fbb1f78116d5f9ecc70b32174aa1b doi: 10.3390/rs13204112

McDermid, S., Nocco, M., Lawston-Parker, P., Keune, J., Pokhrel, Y., Jain, M., ... Yokohata, T. (2023). Irrigation in the earth system. , 1–19. Retrieved 2023-07-02, from https://www.nature.com/articles/s43017-023-00438-5 (Publisher: Nature Publishing Group) doi: 10.1038/s43017-023-00438-5

Neumann, K., Stehfest, E., Verburg, P. H., Siebert, S., Müller, C., & Veldkamp, T. (2011). Exploring global irrigation patterns: A multilevel modelling approach. , *104*(9), 703–713. Retrieved 2025-09-01, from https://www.sciencedirect.com/science/article/pii/S0308521X11001181 doi: 10.1016/j.agsy.2011.08.004

Niu, G.-Y., Yang, Z.-L., Mitchell, K. E., Chen, F., Ek, M. B., Barlage, M., ... Xia, Y. (2011). The community Noah land surface model with multiparameterization options (Noah-MP): 1. Model description and evaluation with local-scale measurements. *Journal of Geophysical Research: Atmospheres*, *116*(D12). doi: 10.1029/2010JD015139

Ozdogan, M., Rodell, M., Beaudoing, H. K., & Toll, D. L. (2010). Simulating the effects of irrigation over the united states in a land surface model based on satellite-derived agricultural data. *Journal of Hydrometeorology*, *11*(1), 171 - 184.

Peters-Lidard, C. D., Houser, P. R., Tian, Y., Kumar, S. V., Geiger, J., Olden, S.,

... others (2007). High-performance earth system modeling with nasa/gsfc's land information system. *Innovations in Systems and Software Engineering*, *3*(3), 157–165.

Purnamasari, D., Teuling, A. J., & Weerts, A. H. (2025). Identifying irrigated areas using land surface temperature and hydrological modelling: application to the rhine basin. *Hydrology and Earth System Sciences*, *29*(6), 1483–1503.

Teluguntla, P., Thenkabail, P., Oliphant, A., Gumma, M., Aneece, I., Foley, D., & McCormick, R. (2023, January). *Landsat-Derived Global Rainfed and Irrigated-Cropland Product 30 m V001.* NASA EOSDIS Land Processes Distributed Active Archive Center (DAAC) data set, DOI: 10.5067/COMMUNITY/LGRIP/LGRIP30.001, id.LGRIP30.001 (2023). doi: 10.5067/COMMUNITY/LGRIP/LGRIP30.001

Torrence, C., & Compo, G. P. (1998). A practical guide to wavelet analysis. , *79*(1), 61–78. Retrieved 2024-11-05, from `https://journals.ametsoc.org/view/journals/bams/79/1/1520-0477_1998_079_0061_apgtwa_2_0_co_2.xml` (Publisher: American Meteorological Society Section: Bulletin of the American Meteorological Society) doi: 10.1175/1520-0477(1998)079⟨0061:APGTWA⟩2.0.CO;2

Zaussinger, F., Dorigo, W., Gruber, A., Tarpanelli, A., Filippucci, P., & Brocca, L. (2019). Estimating irrigation water use over the contiguous united states by combining satellite and reanalysis soil moisture data. , *23*(2), 897–923. Retrieved 2025-09-01, from `https://hess.copernicus.org/articles/23/897/2019/` (Publisher: Copernicus GmbH) doi: 10.5194/hess-23-897-2019